Platform for controllable Majorana zero modes using superconductor/ferromagnet heterostructures

Giorgos Livanas[a,1]**, Nikolaos Vanas**[1]**, Manfred Sigrist**[2]**, Georgios Varelogiannis**[1]

[1]Department of Applied Mathematical and Physical Sciences, NTUA, 15780, Athens, Greece
[2]Institut für Theoretische Physik, ETH, 8093, Zürich, Switzerland

Abstract We propose a novel platform for the creation and manipulation of Majorana zero modes consisting of a ferromagnetic metallic wire placed between conventional superconductors which are in proximity to ferromagnetic insulators. Our device relies on the interplay of applied supercurrents and exchange fields emerging from the ferromagnetic insulators. We assert that the proposed superconductor/ferromagnet heterostructures exhibit enhanced controllability, since topological superconductivity can be tuned apart from gate voltages applied on the ferromagnetic wire, also by manipulating the applied supercurrents and/or the magnetisation of the ferromagnetic insulators.

1 Introduction

Topological quantum computation is the most promising answer to the quantum decoherence problem hindering the development of quantum computers [1]. Topologically protected qubits formed by non-Abelian anyons would allow to store and process quantum information in decoherence-resilient schemes. Majorana zero modes (MZMs) are arguably the most natural realization of such non-Abelian anyons. Indeed, MZMs are expected to emerge at the edges of 1D [2] and at the vortices of 2D [3] topological p-wave superconductors but unfortunately p-wave superconductivity appears to be scarce in nature. However, a topological p-wave superconducting state has been demonstrated to emerge in heterostructures comprising topological insulators and conventional superconductors [4], where proximity induced singlet superconductivity pairs the helical states confined at the boundaries of the topological insulator realising an effectively spinless superconducting state. Following this seminal work numerous proposals have been put forward involving superconductor-semiconductor heterostructures [5,6,7], non-centrosymmetric superconductors [8], surfaces of heavy metals [9], the quantum anomalous Hall state [10] and 2D electron gases

[11]. Key elements for realising effectively spinless superconductivity in all the aforementioned proposals, is spin momentum locking and a Zeeman energy term, thereby many schemes for realising MZMs rely on effective spin orbit coupling emerging from the application of laser beams in ultracold atoms superfluids [12], nanomagnets in superconducting wires [13] or carbon nanoribbons [14], magnetic tunnel junctions in proximized 2D electron gases [15], from the helical ordering of magnetic adatoms embedded in conventional superconductors [16,17,18,19,20] as well as from the curved geometry of carbon nanotubes [21] and semiconducting wires [22] and from the spatially modulated width of planar Josephson junctions [23]. Moreover, in most of the above setups for engineering MZMs, the required Zeeman energy is provided by the application of an external magnetic field. Superconductor/ferromagnet heterostructures (SC-FM) support the emergence of topological superconductivity without the requirement of an external magnetic field, as has been already demonstrated for ferromagnetic metal/superconductor hetero structures with spin active interfaces [24,25] and ferromagnetically aligned magnetic adatoms chains embedded in conventional superconductors with spin orbit coupling [26]. However, the particular ferromagnet-superconductor heterostructures exhibit limited controllability of the emergent MZMs.

[a]e-mail: livanasg@mail.ntua.gr (corresponding author)

Here we propose such a platform for engineering controllable TSC and MZMs based on superconductor/ferromagnet heterostructures and the application of supercurrents and gate voltages. The heterostructures consist of a ferromagnetic metallic wire (FM) placed among conventional superconductors (SCs) which are in proximity to ferromagnetic insulators (FIs) (see Fig. 1). The general underlying mechanism has already been presented in our previous publication [27] and consists of two stages. In the first stage, triplet p-wave correlations are induced in the SCs, due to the coexistence of conventional superconductivity with applied supercurrents and exchange fields emerging from the FIs. As we show below, the d-vector [28] of the induced p-wave correlations is parallel to polarization of the exchange field of the FIs. In the second stage, these p-wave correlations mediate into the FM where an analogous to Kitaev's chain spinless superconducting state is realised provided the magnetisation of the wire and the d-vector of the p-wave correlations are misaligned. We demonstrate that our device platform exhibits enhanced controllability through the externally applied supercurrents and the manipulation of the exchange fields resulting from the FIs, which can be achieved by the use of currents [29] or applied gate voltages [30,31]. We remark that although supercurrents were involved in other proposals for engineering MZMs [32,33,34,35, 36,37], in our device they do not constitute simply an alternative to magnetic fields, but instead they can be also exploited to manipulate the phase of the induced TSC, a property crucial for designing feasible braiding schemes.

2 Induced p-wave superconductivity

Initially, we describe how the coexistence of conventional superconductivity, supercurrents and exchange fields induces triplet p-wave correlations with a d-vector parallel to the polarization of the exchange fields. As we have already pointed out in [27] these four fields or order parameters constitute a quartet [38] meaning that the presence of any three of them induces the missing fourth one. To this end we employ the following Hamiltonian representing a 1D SC,

$$H = \int \Psi^\dagger \left([\frac{\partial_x^2}{2m} + \mu]\tau_z + \tau_z \boldsymbol{h} \cdot \tilde{\boldsymbol{\sigma}} + \Delta \tau_y \sigma_y \right) \Psi \quad (1)$$

where $\Psi^\dagger = (\psi_\uparrow^\dagger, \psi_\downarrow^\dagger, \psi_\uparrow, \psi_\downarrow)$ the extended Nambu spinor and $\boldsymbol{\tau}$ and $\tilde{\boldsymbol{\sigma}} = (\sigma_x, \tau_z\sigma_y, \sigma_z)$ are the Pauli matrices acting on particle-hole and spin space, respectively, $\boldsymbol{h}$ the exchange field and $\Delta = |\Delta|e^{iJx\tau_z}$ the singlet superconducting field which acquires a phase gradient J

proportional to the applied supercurrent density. Under the gauge transformation $\Psi(x) \to e^{-iJ/2x\tau_z}\Psi(x)$ kinetic term $\frac{\partial_x^2}{2m}$ transforms to $\frac{\partial_x^2}{2m} + i\frac{J}{2m}\partial_x - \frac{J^2}{8m}\tau_z$ where $i\frac{J}{2m}\partial_x$ is the velocity corresponding to the supercurrent density and $-\frac{J^2}{8m}\tau_z$ can be absorbed in the chemical potential μ. Thus, Hamiltonian Eq. 1 takes the form $H = \int dx \Psi^\dagger \left([\frac{\partial_x^2}{2m} + \mu]\tau_z + i\frac{J}{2m}\partial_x + \tau_z \boldsymbol{h} \cdot \tilde{\boldsymbol{\sigma}} + |\Delta|\tau_y\sigma_y \right)\Psi$. For periodic boundary conditions, a Fourier transformation to momentum k space leads to the energy bands of the wire $E_{s,\pm}(k) = -sh + \frac{J}{2m}k \pm \sqrt{\left(\frac{k^2}{2m} - \mu\right)^2 + \Delta^2}$, where $s = \pm$, with $+$ and $-$ corresponding to different spin configurations depending on the orientation of the $\boldsymbol{h}$.

For translationally invariant systems, p-wave triplet correlations derive from equation

$$< \Delta_{\boldsymbol{p}} > \propto \frac{1}{\beta} \Sigma_{i\omega_n} Tr\{k\tau_x \boldsymbol{d} \cdot \tilde{\boldsymbol{\sigma}} i\sigma_y \hat{G}(k, i\omega_n)\}, \quad (2)$$

where $\hat{G}(k, i\omega_n)$ the Matsubara Green's function with $\omega_n = (2n+1)\pi/\beta$ the fermion frequencies and $\beta \propto 1/T$ the inverse of temperature. The above expression simplifies to

$$< \Delta_{\boldsymbol{p}} > \propto \sum_k \sum_m n_F(E_m)$$
$$[U(k)^\dagger k\tau_x \boldsymbol{d} \cdot \tilde{\boldsymbol{\sigma}} i\sigma_y U(k)]_{mm}, \quad (3)$$

where m is the energy band index, $U(k)$ the transformation matrix which diagonalises the Hamiltonian matrix $\hat{H}(k)$ while $[]_{mm}$ denotes the m diagonal term of the corresponding matrix. Based on the above analysis it is straightforward to derive the expression

$$< \Delta_{p,\boldsymbol{d}\|\boldsymbol{h}} > \propto \sum_k k \frac{\Delta}{\sqrt{\Delta^2 + (\frac{k^2}{2m} - \mu)^2}} \cdot$$
$$\left[n_F(E_{s,-}) - n_F(E_{s',+}) - [n_F(E_{s',-}) - n_F(E_{s,+})]\right] (4)$$

for the triplet correlations with $\boldsymbol{d} \parallel \boldsymbol{h}$. Since for $h = 0$, $n_F(E_{s,\pm}) = n_F(E_{s',\pm})$, triplet correlations vanish, $< \Delta_{p,d\|\boldsymbol{h}} > = 0$. Similarly, for $J = 0$ we get $< \Delta_{p,d\|\boldsymbol{h}} > = 0$, since the expression $k\left(n_F(E_{s,-}) + n_F(E_{s',+})\right. - [n_F(E_{s,+}) + n_F(E_{s',-})])$ is odd in momenta k. However, when both h and J are finite, both spin and spatial inversion symmetries break, leading to a finite sum for triplet correlations $< \Delta_{p,d\|\boldsymbol{h}} >$. Regarding correlations $< \Delta_{p,d\perp\boldsymbol{h}} >$, matrix $[U(k)^\dagger k\tau_x \boldsymbol{d}_{\perp\boldsymbol{h}} \cdot \tilde{\boldsymbol{\sigma}} i\sigma_y U(k)]$ has no diagonal elements, therefore they vanish. Thus, only when h and J are both finite in a conventional superconductor Δ, $< \Delta_{p,d\|\boldsymbol{h}} >$ correlations are induced.
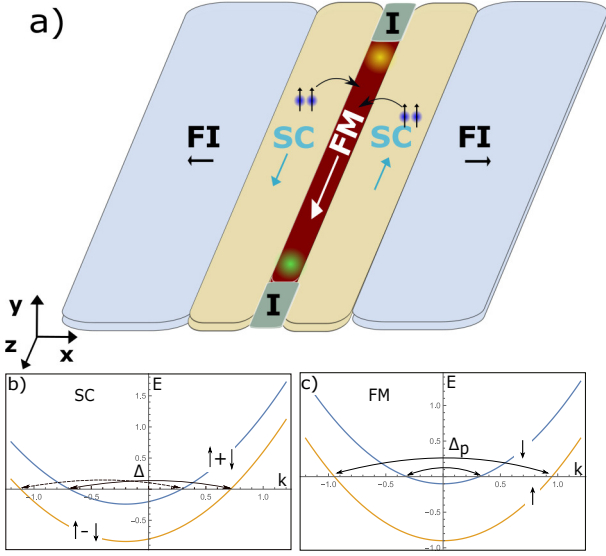
Fig. 1 a) Device for engineering controllable MZMs based on superconductor-ferromagnet heterostructures. A ferromagnetic metallic wire (FM) is placed between two conventional superconductors (SCs) where supercurrents (blue arrows) are applied in an anti-parallel configuration. Exchange fields are induced in the SCs due to proximity with the ferromagnetic insulators (FIs). The optimal configuration is when the magnetisations of the FIs (black arrows) is perpendicular to that of the FM (white arrow) and anti-parallel with each other. The application of supercurrent J and exchange field h_x in the SC induces an equal spin triplet pairing component (blue dots) which mediates in the FM resulting in the emergence of MZMs $\gamma_a = (\psi^\dagger + \psi)$ (yellow dot) and $\gamma_b = i(\psi^\dagger - \psi)$ (green dot) at the edges of the wire. b) The energy bands of a system with an applied current J and a h_x exchange field. The singlet superconducting field Δ pairs electron from different bands. The application of J and h_x results in an imbalance of singlet pairing between the two spin configurations, and therefore an equal spin triplet pairing component is induced. However, the induced triplet superconducting field still pairs electrons from different bands. c) The induced equal spin triplet superconducting correlations Δ_p mediate in the FM where an exchange field h_z is present. In the spin configuration of the energy bands of FM, Δ_p pairs electrons of the same band, i. e. intraband pairing, realising an effectively spinless superconducting state.

From Eq. 4 it becomes apparent that $< \Delta_{p,d\|\boldsymbol{h}} >$ correlations emerge from the imbalance among the two configurations $\psi^\dagger_{k,s}\psi^\dagger_{-k,s'}$ and $\psi^\dagger_{k,s'}\psi^\dagger_{-k,s}$ of the interband singlet pairing (See Sup. Mat.). Moreover, since $J \to -J$ leads to $E_{s,\pm}(k) \to E_{s,\pm}(-k)$ we get $< \Delta_{p,d\|\boldsymbol{h}} > \to - < \Delta_{p,d\|\boldsymbol{h}} >$ or equivalently the phase of the triplet order parameter changes by π. Most importantly, there are no threshold values for h and J in order for $< \Delta_{p,\boldsymbol{d}\|\boldsymbol{h}} >$ correlations to be induced. Therefore the particular mechanism is valid even for small values of these parameters which leave conventional superconductivity unaffected.

3 Topological superconductivity in superconductor-ferromagnet heterostructures

Evidently, topological superconductivity cannot be realised simply by applying a supercurrent in a superconducting wire under the presence of an exchange field, since the emergent triplet pairing correlations are parallel to the polarization of the exchange field and therefore connect different energy bands of the wire, i.e. we get interband triplet pairing. In order to realise MZMs we need intraband superconductivity. In our device intraband superconductivity emerges in the FM where the triplet correlations induced in the conventional SCs mediate by means of the proximity effect. Necessary condition for the emergence of intraband superconductivity is that the exchange field h of the wire and the $\boldsymbol{d}$ vector of the induced triplet correlations are misaligned. Therefore, a topological superconducting state is realised in a FM separating two conventional SCs when supercurrents are applied in an antiparallel configuration and the exchange fields are perpendicular to the magnetisation of the wire and antiparallel to each other (see Fig. 1). The antiparallel configuration guarantees that the supercurrent and the exchange field vanish into the wire and therefore no $< \Delta_{p,d\|\boldsymbol{h}_{FM}} >$ correlations are induced there. Although this is the optimal configuration, we show that TSC is realised even for small misalignment angles among the magnetisations of the FM and the FIs and even for not exactly anti-parallel supercurrents and exchange fields (see Fig: 2).

In order to illustrate numerically the above arguments we employ a lattice Bogoliubov de Gennes equation, $\mathcal{H} = \sum_{\boldsymbol{i},\boldsymbol{j}} \Psi^\dagger_{\boldsymbol{i}} \hat{H}_{\boldsymbol{i},\boldsymbol{j}} \Psi_{\boldsymbol{j}}$, which describes the SC-FM-SC presented in Fig. 1. The lattice Hamiltonian consists of three parts which describe each region of the heterostructure separately and a corresponding coupling Hamiltonian. In particular, we have

$$\mathcal{H} = [H_{l,SC} + H_{l,tc} + H_{FM} + H_{r,tc} + H_{r,SC}], \quad (5)$$

where

$$H_{a,SC} = \sum_{\boldsymbol{i},\boldsymbol{j}} \Psi^\dagger_{a,\boldsymbol{i},SC} \left[(tf_{\boldsymbol{i},\boldsymbol{j}} + \mu_{SC})\tau_z + h_{a,SC}\tau_z\sigma_x \right.$$
$$\left. + \Delta\tau_y\sigma_y + J_{a,SC}g^z_{\boldsymbol{i},\boldsymbol{j}} \right] \Psi_{a,\boldsymbol{j},SC} \quad (6)$$

the Hamiltonian of the superconductor, with $a = l, r$ for the left and right SC respectively, and $h_{l,SC} = -h_{r,SC}$, $J_{l,SC} = -J_{r,SC}$, while

$$H_{FM} = \sum_{\boldsymbol{i,j}} \Psi_{\boldsymbol{i},FM}^{\dagger} \left[(tf_{\boldsymbol{i,j}} + \mu_{FM})\tau_z + h_{FM}\tau_z\sigma_z \right] \Psi_{\boldsymbol{j},FM} \tag{7}$$

the 1D Hamiltonian of the FM wire. We remark that part $H_{a,SC}$ of the Hamiltonian Eq. 5 is the lattice counterpart of Hamiltonian Eq. 1 extended in two dimensions. We have introduced the Nambu spinors $\Psi_{a,\boldsymbol{i},SC}^{\dagger} = (\psi_{a,\uparrow,\boldsymbol{i}}^{\dagger}, \psi_{a,\downarrow,\boldsymbol{i}}^{\dagger}, \psi_{a,\uparrow,\boldsymbol{i}}, \psi_{a,\downarrow,\boldsymbol{i}})$ and $\Psi_{\boldsymbol{i},FM}^{\dagger} = (\psi_{\uparrow,\boldsymbol{i}}^{\dagger}, \psi_{\downarrow,\boldsymbol{i}}^{\dagger}, \psi_{\uparrow,\boldsymbol{i}}, \psi_{\downarrow,\boldsymbol{i}})$, where $\psi_{a,s,\boldsymbol{i}}^{(\dagger)}$ creates (destroys) an electron with spin s at lattice site $\boldsymbol{i}$ in the a SC, while $\psi_{s,\boldsymbol{i}}^{(\dagger)}$ creates(destroys) an electron with spin s at lattice site $\boldsymbol{i}$ in the FM wire. We have also employed the Pauli matrices $\boldsymbol{\tau}$ and σ acting on particle-hole and spin space respectively, and the functions $f_{\boldsymbol{i,j}} = \delta_{\boldsymbol{j,i\pm\hat{x}}} + \delta_{\boldsymbol{j,i\pm\hat{z}}}$ and $\boldsymbol{g_{i,j}} = (g_{\boldsymbol{i,j}}^x, g_{\boldsymbol{i,j}}^z) = (\pm i\delta_{\boldsymbol{j,i\pm\hat{x}}}, \pm i\delta_{\boldsymbol{j,i\pm\hat{z}}})$, even and odd in spatial inversion, connecting nearest neighbours lattice points. Moreover, t is the hopping integral, μ_{SC} and μ_{FM} the chemical potential in the superconducting regions and the ferromagnetic wire respectively, while $h_{a,SC}$ and h_{FM} are the corresponding exchange fields. Moreover, we include the conventional superconducting field Δ and the supercurrent density term $J_{a,SC}$. The SCs are connected with the FM wire through the following coupling Hamiltonian

$$H_{a,tc} = \sum_{\boldsymbol{i,j},s} t_c \psi_{a,\boldsymbol{i,j},s}^{\dagger} \psi_{\boldsymbol{i,j},s} + H.c.. \tag{8}$$

The proximity to the FIs is modelled by considering the finite exchange fields $h_{a,SC}$ over the SC regions emerging from the interfacial exchange interaction between the localized magnetic moments of the FIs and the SCs conduction band electrons. The dependence of the emerging MZMs on the width of the conventional superconductors eludes this simplified model and will be examined in a more detailed work. However, the width of the conventional superconductors along the x-axis is not important when the FIs are deposited on top or below the SCs. MZMs are anticipated to emerge localised at the edges of the wire for $|2t - \sqrt{(h_{FM})^2 - \Delta'^2}| < |\mu_{FM}| < |2t + \sqrt{(h_{FM})^2 - \Delta'^2}|$ where Δ' is the induced by proximity singlet superconducting field over the FM [27]. From Fig. 2a we conclude that the hopping term along the wire is renormalised to $t' \simeq 0.85t$, due to the coupling of the wire to the SCs [39]. Figs. 2 b),c) and d) demonstrate the significant robustness of our device against deviations from the optimal antiparallel alignment of the magnetisation in the FIs and the antiparallel configuration of the supercurrents in the SCs.
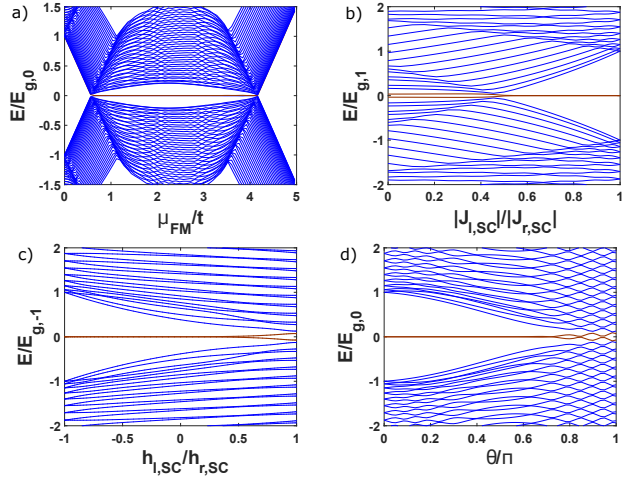

Fig. 2 a) The low energy spectrum of the device as a function of the chemical potential of the wire μ_{FM}/t, where $\Delta/t = 0.5$, $\mu_{SC}/t = 0$, $|J_{SC}|/t = 0.2$ and $|h_{SC}|/t = 0.2$. Eigenenergies are normalised with respect to energy gap $E_{g,0}$ for $\mu_{FM} = 0$ and $h_{FM}/t = 2.4$. b) The energy gap in the wire for $h_{FM}/t = \mu_{FM}/t = 2.4$ with respect to the ratio of the magnitude of the supercurrents $|J_{l,SC}|,|J_{r,SC}|$ in the left and the right SC, respectively. The supercurrents flow in the opposite direction. The energy spectrum is normalised to the energy gap $E_{g,1}$ corresponding to $J_{l,SC} = -J_{r,SC}$. c) Low energy excitation spectrum as a function of the ratio $h_{l,SC}/h_{r,SC}$ of the exchange fields along the x-axis in the left and right SC. The antiparallel configuration leads to the maximum energy gap. d) The dependence of the excitation spectrum on the rotation angle θ of $h_{r,SC}$ over the right SC in the $x - z$ plane, where for $\theta = 0$, $h_{r,SC} = -h_{l,SC}$ along the x-axis. Energies in c) are normalised to $E_{g,-1}$ corresponding to $h_{l,SC} = -h_{r,SC}$, while in d) are normalised to $E_{g,0}$ for $\theta = 0$. The device appears to be more robust against deviations from the optimal anti-parallel configuration of the exchange fields.

4 Controlling Majorana zero modes

To demonstrate the controllability of our setup we consider a junction between two ferromagnetic wires FM1 and FM2 as depicted in Fig. 3. The conventional superconductors in this configuration are separated by an insulator in order for the supercurrents adjacent of FM1 and FM2 to be controlled independently. First, we consider a sinusoidal variation $J = J_0 \cos(\phi)$ of the magnitude of the supercurrents applied in the SCs that are adjacent to the FM2, where ϕ is just a parameter without any physical meaning. The supercurrents always flow in opposite directions. In Fig. 3 is presented the supercurrents configuration for $\phi = \pi$ while in Fig. 4a) is shown the low-energy spectrum of this junction with respect to parameter ϕ. The FM wires are coupled through the insulating region with a hopping term $t_c = 0.5t$. For $-\pi/2 < \phi < \pi/2$, the superconducting states in the two FMs acquire the same phase (0- Josepshon junction) and MZMs $\gamma_{1,b}$ localised in the right edge of FM1

and $\gamma_{2,a}$ localised at the left edge of the FM2 interact with each other giving rise to an ordinary fermionic state with finite energy. The other two MZMs $\gamma_{1,a}$ at the left edge of FM1 and $\gamma_{2,b}$ at the right edge of FM2 remain unpaired and therefore stick at zero energy. For $\phi = \pm\pi/2$ the energy gap in FM2 closes and MZMs $\gamma_{2,a}$ and $\gamma_{2,b}$ fuse, while $\gamma_{1,a}$ and $\gamma_{1,b}$ remain uncoupled. Remarkably for $\pi/2 < \phi < 3\pi/2$, for which the supercurrent flow is reversed on both sides of FM2, *the phase of the induced p-wave superconductivity in FM2 changes by π leading to the formation of a π-Josepshon junction* among the FM wires. The reversal of the flow of the supercurrent leads to an *interchange of the position of $\gamma_{2,a}$ and $\gamma_{2,b}$*. Since in our case Majorana operators, γ_b and γ_a have opposite time-reversal T parities, $T\gamma_a T^{-1} = \gamma_a$ while $T\gamma_b T^{-1} = -\gamma_b$, the coupling term $i\gamma_{1,b}\gamma_{2,b}$ is odd in time-reversal [40]. However, in our setup the two FM wires are only coupled by the even in time-reversal t_c hopping term. Thus, $\gamma_{2,b}$ cannot couple with $\gamma_{1,b}$ and the heterostructure hosts in this case four MZMs reflected in the low-energy quasi-particle spectrum. Note on the same figure that the four MZMs are stabilised even for very small values of the supercurrent.
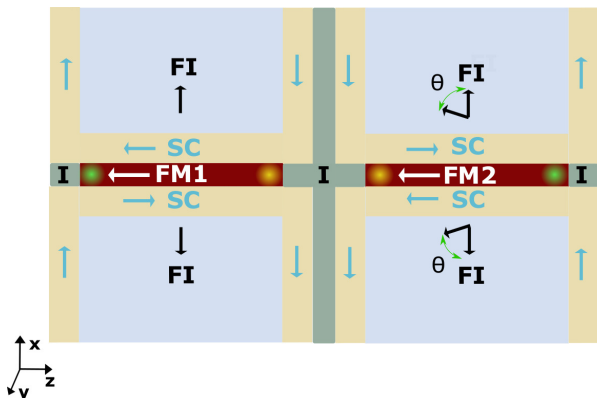

Fig. 4 Low-energy quasiparticle energy spectrums for the setup presented in Fig. 3, a) with respect to parameter ϕ controlling the supercurrents ($J = J_0 \cos(\phi)$) in the conventional SCs adjacent to FM2 and b) with respect to θ corresponding to the angle of FIs magnetisation in the x-z plane. We remark that $\theta = 0$ in a), while $\phi = 0$ in b). Eigenenergies are normalised to the energy gap $E_{gap,\pi}$ for $\phi = \pi$ and $\theta = \pi$ respectively. The second lowest eigenenergy (black line) is multiplied by 10 to demonstrate clearly the splitting of the MZMs. The spectral function $|\Psi|_z^2$ of the two lowest eigenenergies of the heterostructure, c) for $\theta = 0.45\pi$ and d) for $\theta = 0.55\pi$. The particular angles are indicated in figure b) by the dashed red line. The function is normalised to the maximum value $|\Psi|_{max}^2$. For $\theta = 0.45\pi$, MZMs localised in the right edge of FM1 and left edge of FM2 form a fermionic state with finite energy $E/t = 0.03$. For $\theta = 0.55\pi$, four MZMs emerge. Since in FM2 the FIs magnetisation is not in the optimal anti-parallel configuration, MZMs appear to be less localised. In the upper c) plot the left and the right part of the function is normalised independently in order to compare the localisation length of MZMs in the two FMs.

Fig. 3 Setup of two ferromagnets (FMs) separated by an insulator (I) in proximity with conventional superconductors (SCs) and ferromagnetic insulators (FIs). The junction is controlled by varying the supercurrents (blue arrows) and/or rotating the magnetisation (black arrow) of the FIs adjacent to FM2 by angle θ.

Next we investigate the same junction by rotating the magnetisation and therefore the exchange field of the FIs adjacent to FM2, in the x-z plane, $h = h_z \sin(\theta) + h_x \cos(\theta)$ where θ is the angle from the x-axis. Since we require that the x component of the exchange fields of FIs adjacent to FM2, point at the opposite direction for every θ, the magnetisation in the upper FI rotates clockwise while in the lower FI rotates counter-clockwise (Fig.3). The supercurrent in the two FMs flows along the same direction, therefore for $\theta = 0$
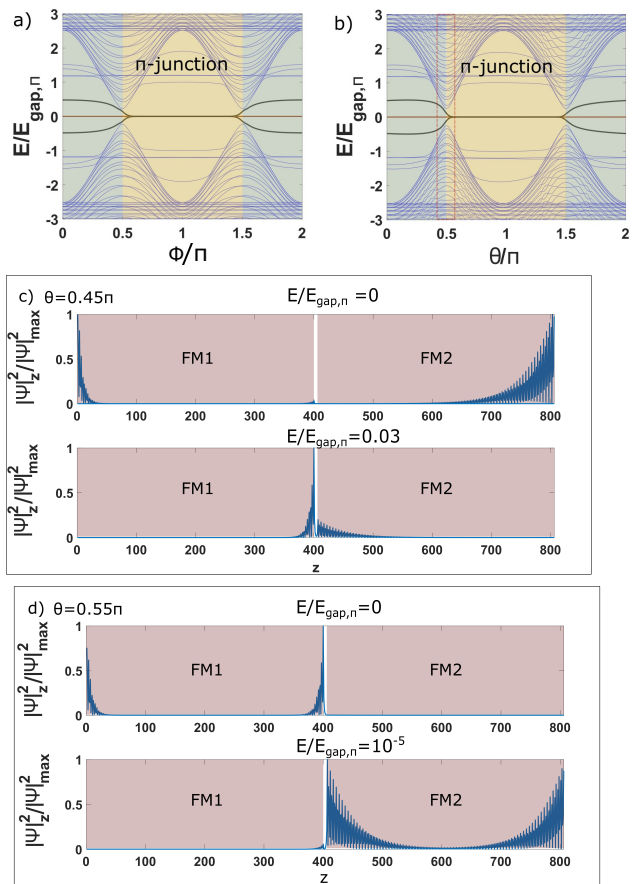
the junction is formed by two identical copies of FMs embedded in conventional SCs. According to our mechanism topological SC emerges only when the magnetisation of the FIs and that of the ferromagnetic wire is misaligned. Indeed, for $\theta = \pi/2$ the energy gap at the wire closes (Fig. 4b)). Remarkably for $\pi/2 < \theta < 3\pi/2$ for which the x component of the magnetisation of the

FIs adjacent to FM2 is opposite to that of the FIs adjacent to FM1, *a π-Josepshon junction is formed* and four Majorana zero modes emerge localised at the edges of the two wires. In Fig. 4c) we display the spectral function $|\Psi|_z^2$ along the z-axis over the FM wires, where $\hat{\mathcal{H}}\Psi = E\Psi$, with Ψ corresponding in this context, to the wavefunction of the eigenstates of the two lowest eigenvalues for $\theta = 0.45\pi$ and $\theta = 0.55\pi$. We remark, that small rotations of the FIs magnetisation can be achieved by the application of gate voltages [30,31].

5 Conclusions

We present a novel device platform for engineering MZMs based on SC-FM heterostructures. Key elements of the underlying mechanism are the externally applied supercurrents and the emergent exchange fields, due to proximity of the SCs with FIs. Developments in the fabrication of SC-FI heterostructures [41] and ferromagnetic metallic Co [42,43] or Fe [44] nanowires embedded in conventional SCs, enhance the experimental feasibility of our proposal. Several works have demonstrated both theoretically [45,46] and experimentally [47,48, 49] the emergence of exchange fields in conventional SCs in proximity to FIs, e.g. in EuS/Al and EuO/Al heterostructures. Finally, our platform does not require externally applied magnetic fields, yet it facilitates the control of the emergent MZMs, either through the applied supercurrents or the manipulation of FIs magnetisation by use of currents or applied gate voltages. In this way we circumvent the screening effects problem [50] that undermines schemes for braiding MZMs based on semiconductors [51].

Author contribution statement Dr. Giorgos Livanas has conducted the analysis and wrote the initial version of the manuscript, Nikos Vanas contributed to numerical calculations, Prof. Giorgos Varelogiannis and Prof. Manfred Sigrist have revised and wrote the final version of the manuscript. The work was conceptualized by Dr. Giorgos Livanas and Prof. Giorgos Varelogiannis.

References

1. C. Nayak, S. H. Simon, A. Stern, M. Freedman, and S. Das Sarma, Non-Abelian anyons and topological quantum computation, Rev. Mod. Phys. 80, 1083 (2008).
2. A.Y. Kitaev, Unpaired Majorana fermions in quantum wires, Phys.-Usp. **44**, 131-136 (2001).
3. D.A. Ivanov, Non-Abelian Statistics of Half-Quantum Vortices in p-Wave Superconductors, Phys. Rev. Lett. **86**, 268 (2001).
4. Liang Fu and C. L. Kane, Superconducting Proximity Effect and Majorana Fermions at the Surface of a Topological Insulator, Phys. Rev. Lett. 100, 096407 (2008).
5. Sau, J. D., Lutchyn, R. M., Tewari, S. and Sarma, S. D., Generic new platform for topological quantum computation using semiconductor heterostructures, Phys. Rev. Lett. **104**, 040502 (2010).
6. J. Alicea, Majorana fermions in a tunable semiconductor device, Phys. Rev. B **81**, 125318 (2010).
7. J. Linder and A. Sudbo, Majorana fermions manifested as interface states in semiconductor hybrid structures, Phys. Rev. B 82, 085314 (2010).
8. P. Ghosh, J. D. Sau, S. Tewari, S. Das Sarma, Non-Abelian topological order in noncentrosymmetric superconductors with broken time-reversal symmetry, Phys. Rev. B **82**, 184525 (2010).
9. C. Potter, P. A. Lee, Topological superconductivity and Majorana fermions in metallic surface states, Phys. Rev. B **85**, 094516 (2012).
10. X. L. Qi, T. L. Hughes, Zhang SC., Chiral topological superconductor from the quantum Hall state, Phys. Rev. B **82**, 184516 (2010).
11. M. Hell, M. Leijnse, and K. Flensberg, Two-Dimensional Platform for Networks of Majorana Bound States, Phys. Rev. Lett. 118, 107701 (2017).
12. S. L. Zhu, L. B. Shao, Z. D. Wang, L. M. Duan, Probing Non-Abelian Statistics of Majorana Fermions in Ultracold Atomic Superfluid, Phys. Rev. Lett. 106, 100404 (2011).
13. M. Kjaergaard, K. Wolms, K. Flensberg, Majorana fermions in superconducting nanowires without spin-orbit coupling, Phys. Rev. B 85, 020503 (2012).
14. J. Klinovaja and D. Loss, Giant Spin-Orbit Interaction Due to Rotating Magnetic Fields in Graphene Nanoribbons, Phys. Rev. X 3, 011008 (2013).
15. A. Matos-Abiague et al., Tunable magnetic textures From Majorana bound states to braiding, Solid State Commun. 262, 1 (2017).
16. T. P. Choy, J. M. Edge, A. R. Akhmerov, C. W. J. Beenakker, Majorana fermions emerging from magnetic nanoparticles on a superconductor without spin-orbit coupling, Phys. Rev. B 84, 195442 (2011).
17. F. Pientka, L. I. Glazman, F. von Oppen, Topological superconducting phase in helical Shiba chains, Phys. Rev. B 88, 155420 (2013).
18. J. Klinovaja, P. Stano, A. Yazdani, D. Loss, Topological Superconductivity and Majorana Fermions in RKKY Systems, Phys. Rev. Lett. 111, 186805 (2013).
19. M. M. Vazifeh, M. Franz, Self-Organized Topological State with Majorana Fermions, Phys. Rev. Lett. 111, 206802 (2013).
20. M. Schecter, K. Flensberg, M. H. Christensen, B. M. Andersen, and J. Paaske Self-organized topological superconductivity in a Yu-Shiba-Rusinov chain, Phys. Rev. B 93, 140503 (2016).
21. J. D. Sau, S. Tewari, Topological superconducting state and Majorana fermions in carbon nanotubes, Phys. Rev. B 88, 054503 (2013).

22. T. Ojanen, Majorana states and devices in magnetic structures, Phys. Rev. B 88, 220502 (2013).

23. P. P. Paudel, T. Cole, B. D. Woods, and T. D. Stanescu, Enhanced topological superconductivity in spatially modulated planar Josephson junctions Phys. Rev. B 104, 155428 (2021).

24. S. B. Chung, H .J. Zhang, X. L. Qi, Zhang SC, Topological superconducting phase and Majorana fermions in half-metal/superconductor heterostructures, Phys. Rev. B 84, 060510 (2011).

25. S. Takei, V. Galitski, Microscopic theory for a ferromagnetic nanowire/superconductor heterostructure: Transport, fluctuations, and topological superconductivity, Phys. Rev. B 86, 054521 (2012).

26. S. Nadj-Perge, I. K. Drozdov, B. A. Bernevig, A. Yazdani, Proposal for realizing Majorana fermions in chains of magnetic atoms on a superconductor, Phys. Rev. B 88, 020407 (2013).

27. G. Livanas, M. Sigrist and G. Varelogiannis, Alternative paths to realize Majorana Fermions in Superconductor-Ferromagnet Heterostructures, Sci Rep 9, 6259 (2019).

28. M. Sigrist and K. Ueda, Phenomenological theory of unconventional superconductivity, Rev. Mod. Phys. 63, 239 (1991)

29. C. Avci, A. Quindeau, CF. Pai, et al., Current-induced switching in a magnetic insulator, Nature Mater 16, 309 (2017).

30. D. Chiba, M. Sawicki, Y. Nishitani, et al., Magnetization vector manipulation by electric fields, Nature 455, 515 (2008).

31. D. Chiba, Y. Nakatani, F. Matsukura, and H. Ohno, Simulation of magnetization switching by electric-field manipulation of magnetic anisotropy, Appl. Phys. Lett. 96, 192506 (2010).

32. A. Romito, J. Alicea, G. Refael, and F. von Oppen, Manipulating Majorana fermions using supercurrents, Phys. Rev. B 85, 020502(R) (2012).

33. A. Heimes, P. Kotetes, G. Schon, Majorana fermions from Shiba states in an antiferromagnetic chain on top of a superconductor, Phys. Rev. B 90, 060507 (2014).

34. O. Dmytruk, M. Thakurathi, D. Loss and J. Klinovaja, Majorana bound states in double nanowires with reduced Zeeman thresholds due to supercurrents, Phys. Rev. B 99, 245416 (2019).

35. O. Lesser, K. Flensberg, F. von Oppen, and Y. Oreg, Three-phase Majorana zero modes at tiny magnetic fields, Phys. Rev. B 103, L121116 (2021).

36. Joel Röntynen and Teemu Ojanen,Tuning topological superconductivity in helical Shiba chains by supercurrent, Phys. Rev. B 90, 180503(R) (2014).

37. André Melo, Sebastian Rubbert, Anton R. Akhmerov, SciPost Phys. 7, 039 (2019) Supercurrent-induced Majorana bound states in a planar geometry, SciPost Phys. 7, 039 (2019).

38. G. Varelogiannis, General Rule Predicting the Hidden Induced Order Parameters and the Formation of Quartets and Patterns of Condensates, arXiv1305.2976 (2013).

39. Y. Peng, F. Pientka, L.I. Glazman and F. von Oppen, Strong Localization of Majorana End States in Chains of Magnetic Adatoms, Phys. Rev. Lett. 114, 106801 (2015).

40. L. Fidkowski and A. Kitaev, Topological phases of fermions in one dimension, Phys. Rev. B 83, 075103 (2011).

41. Y. Liu, S. Vaitiekėnas, S. Martí-Sánchez, C. Koch, S. Hart, Z. Cui, T. Kanne, S. A. Khan, R. Tanta, S. Upadhyay, M. E. Cachaza, C. M. Marcus, J. Arbiol, K. A. Moler, and P. Krogstrup, Semiconductor–Ferromagnetic Insulator–Superconductor Nanowires: Stray Field and Exchange Field, Nano Lett. 2020, 20, 1, 456–462 (2019).

42. M. Giroud, H. Courtois, K. Hasselbach, D. Mailly, and B. Pannetier, Superconducting proximity effect in a mesoscopic ferromagnetic wire, Phys. Rev. B 58, R11872(R) (1998).

43. J. Wang, M. Singh, M. Tian, et al., Interplay between superconductivity and ferromagnetism in crystalline nanowires, Nature Phys 6, 389–394 (2010).

44. B. Jäck, Y. Xie, J. Li, S. Jeon, B. A. Bernevig, A. Yazdani, Observation of a Majorana zero mode in a topologically protected edge channel, Science 364, 6447 (2019).

45. T. Tokuyasu, J. A. Sauls, and D. Rainer, Proximity effect of a ferromagnetic insulator in contact with a superconductor, Phys. Rev. B 38, 8823 (1988).

46. Alberto Hijano, Stefan Ilić, Mikel Rouco, Carmen González-Orellana, Maxim Ilyn, Celia Rogero, P. Virtanen, T. T. Heikkilä, S. Khorshidian, M. Spies, N. Ligato, F. Giazotto, E. Strambini, and F. Sebastián Bergeret, Coexistence of superconductivity and spin-splitting fields in superconductor/ferromagnetic insulator bilayers of arbitrary thickness, Phys. Rev. Research 3, 023131 (2021).

47. P. M. Tedrow, J. E. Tkaczyk, and A. Kumar,Spin-Polarized Electron Tunneling Study of an Artificially Layered Superconductor with Internal Magnetic Field: EuO-Al, Phys. Rev. Lett. 56, 1746 1986.

48. X. Hao, J. S. Moodera, and R. Meservey, Spin-filter effect of ferromagnetic europium sulfide tunnel barriers, Phys. Rev. B 42, 8235 (1990).

49. E. Strambini, V. N. Golovach, G. De Simoni, J. S. Moodera, F. S. Bergeret, and F. Giazotto, Revealing the magnetic proximity effect in EuS/Al bilayers through superconducting tunneling spectroscopy, Phys. Rev. Materials 1, 054402, (2017).

50. A. Vuik, D. Eeltink, A. R. Akhmerov and M. Wimmer, Effects of the electrostatic environment on the Majorana nanowire devices, New J. Phys. 18, 03301, (2016).

51. J. Alicea, Y. Oreg, G. Refael, F. von Oppen and M. P. A. Fisher, Non-Abelian statistics and topological quantum information processing in 1D wire networks, Nature Physics 7, pages 412–417 (2011).